NUMERICAL STUDY OF EFFECT OF HANGAR MODIFICATION ON SHIP-AIRWAKE AND HELICOPTER DOWNWASH INTERACTION

Sumit Kumar, oe17s018@smail.iitm.ac.in, Indian Institute of Technology Madras (India)

R. Vijayakumar, vijay2028@iitm.ac.in, Indian Institute of Technology Madras (India)

Abstract

Numerical investigation of the effects of installing a rotating cylinder at the hangar top edge of a frigate on the dynamic interaction between the airwake generated by a Simplified-Frigate-Ship (SFS) during its propulsion and downwash formed by a 3-bladed helicopter rotor trying to perform landing/take-off operations on the flight deck of SFS is undertaken. The SFS hangar is attached with this rotating cylinder to suffice as an active flow device and the flow field so created by this dynamic interaction is analyzed and compared. The modified frigate is modeled using a scale ratio of 1:100. Measurements are taken in terms of rotor thrust coefficient, recirculation length and turbulence intensity at identified locations. STAR CCM+ code that uses FVM (Finite Volume Method) solver to solve the RANS (Reynolds-Averaged-Navier-Stokes) equation along with two-equation $k{-}\omega$ turbulence model as a CFD tool are used for carrying out this numerical analysis. Firstly, the airflow analysis is carried out for SFS-2 in isolation in order to establish a baseline understanding of flow followed by airflow analysis for modified SFS-2, the one equipped with a rotating cylinder. Further, simulations for studying the dynamic interface of ship airwake and the rotor downwash are carried out which involve both the helicopter rotor with ROBIN fuselage and SFS-2 in the first case while the helicopter rotor with ROBIN fuselage and SFS-2 modified with rotating cylinder in the second case. These simulations were varied based upon three distinct cylinder diameter to hangar height ratios for each one of the two rotor hovering -planes positioned parallel to eachother. The inference obtained from this study is that the hangar with a rotating cylinder gives better flow field in terms of recirculation length and thrust co-efficient with zero WOD (wind over deck angle).

1. INTRODUCTION

The Wehrmacht for the first time attempted ship-based helicopter operation during the Second World War in the Baltic Sea. In 1945, US Army converted the helicopter operation vessels into floating repair depots which had special landing platforms to occupy Sikorsky R-4 helicopters [1]. It's been seven decades since the first ship-based helicopter operation was carried out but still even for trained and experienced pilots, the take-off and landing operations of shipborne helicopters is a very challenging task. The primary reason for this is accommodation of a very small confined area behind the ship hangar as compared to that of the wide fields in case of land operations and secondly, the flight deck is in a continuous state of motion relative to the sea. Along with its motion in sea-way, a complex airwake over helo-deck created by the presence of superstructure in front of landing platform poses difficulties to the pilot in performing Helicopter Operations on Ship (HELO).

The ship airwake is considered as a crucial factor in limiting these operations due to the large velocity gradients associated with it and the region of turbulence created thereby. Because of the hanger shape in frigates, there is a large region of eddies formed behind the hangar on the flight deck due to the ship propulsion alone. These eddies during HELO combines with the turbulence generated by the helicopter rotor, ultimately increasing the pilot's workload and reducing the handling capability of the rotorcraft.

The key factors involved in such a dynamic interaction are vortices of different scales that are formed as airflow passes over the ship superstructure and unstable shear layers resulting from the flow separation right at the top edge of the hangar [2,3] as shown in figure 1. These coherent turbulent structures travels downstream interacting with each other thereby forming a highly complex air-wake region over the flight deck [4].

Presented at 45th European Rotorcraft Forum, Warsaw, Poland, 17-20 September, 2019

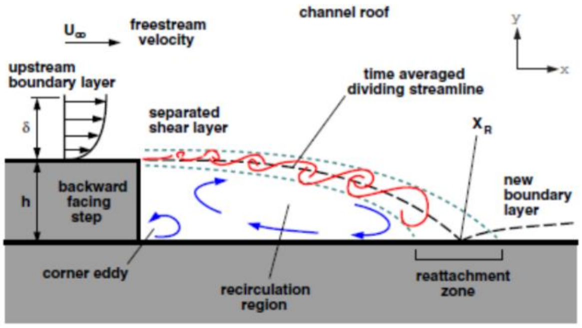

Figure 1 Flow behind the backward-facing step [5]

This highly turbulent flow of air induces large disturbances in the rotor load as well as response during HELO [6].

Other factors leading to difficulties in landing the helicopter on the frigate are rough sea, unwanted gusts around the ship, lightning, etc [7].

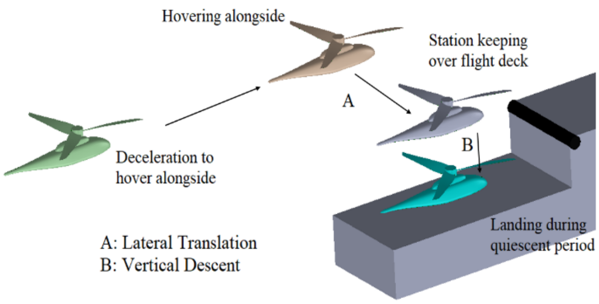

Figure 2 Schematic sketch of the landing approach technique [8]

A ship-borne helicopter landing process in general consists of a lateral translation (i.e. A) and a vertical descent (i.e. B) as shown in Figure 2 [6,8]. The turbulent airwake and recirculation flow regimes that are earlier referred to, plays a vital role in vertical descent phase and can impose disturbances in performing the landing operations. Hence, to carry out safe helicopter operations on the flight deck on a frigate, it is very important to have a better knowledge of airflow around the ship and through the helicopter's rotor. An understanding of the problem associated with the Dynamic Interface (DI) which in maritime terminology refers to take-off and recovery operations of a helicopter on a moving platform i.e. flight deck is also essential in order to find an efficient solution to it [9].

HELO results into changes in the surrounding airflow which in turn also give varied thrust to the helicopter. The value of this thrust depends upon the shape of the hindrance that is the hangar and properties of any active control devices if used. Study of such a case where there are a number of modifications made in the hangar shape only to observe the changes in airflow has been conducted [10,11,12]. On the other hand, the current study focuses on the results obtained by analyzing the active method of turbulent airflow control and its effects on the turbulent intensity, recirculation length and finally on the thrust coefficient of the rotor. Moreover, by installing a rotating cylinder at the hangar top edge, there is a smooth gradual pressure change in the helicopter operating area, avoiding the strong vortices and the shear layer resulting from the sudden change of velocity so as to optimize the ship hangar design.

2. NUMERICALMETHODOLOGY FOR TWO-WAY COUPLED SIMULATION

2.1. CFD and Mathematical Method

The commercial CFD software STAR CCM+ is used to perform the computations wherein Reynolds-averaged-Navier-Stokes (RANS) equation is used to solve the ship-helicopter coupled flow field. The position of rotor for each simulation relative to the hangar is fixed (figure 8). The boundary conditions applied for the velocity of air at the inlet surface simulates the forward motion of the ship and the rotor so that the center of rotation of rotor remains fixed.

The RANS solver used here, reduces the computational effort of the simulations. In simulating the unsteady characteristics of ship airwake the RANS solver is not as satisfactory as Detached Eddy Simulation (DES) and Large Eddy Simulation (LES) solvers but the reality level of RANS solver for the airwake determination is regarded as acceptable. In addition, another numerical study for the airwake of LHA ship model has been carried out by Polsky and Bruner (2001), using both the RANS (using SST $k-\omega$ turbulence model) and Monotone Integrated Large Eddy Simulation (MILES) methods. The result also indicates that the URANS is capable of capturing the unsteady flow field characteristics. As a result, the two-equation $k-\omega$ turbulent model is employed in the current study for RANS closure [6,13]. The RANS equation with SST $k-\omega$ turbulence model is as given below :

Continuity Equation:

$$\rho \frac{\partial u_i}{\partial u_j} = 0 \qquad (1)$$

Navier-Strokes Equation:

$$\rho \frac{\partial}{\partial x_j}\left(\overline{\rho u_i u_j}\right) = -\frac{\partial \bar{p}}{\partial x_i} + \frac{\partial \bar{\sigma}_{ij}}{\partial x_j} \qquad (2)$$

where,

$$\bar{\sigma}_{ij} = \overline{\mu\left(\frac{\partial u_i}{\partial x_j} + \frac{\partial u_j}{\partial x_i}\right)}$$

Turbulent Kinetic Energy:

$$\frac{\partial k}{\partial t} + U_j \frac{\partial k}{\partial x_j} = P_k - \beta^* k\omega + \frac{\partial}{\partial x_j}\left[(v + \sigma_k v_T)\frac{\partial k}{\partial x_j}\right] \qquad (3)$$

Specific dissipation rate:

$$\frac{\partial \omega}{\partial t} + U_j \frac{\partial \omega}{\partial x_j} = \alpha S^2 - \beta\omega^2 + \frac{\partial}{\partial x_j}\left[(v + \sigma_\omega v_T)\frac{\partial \omega}{\partial x_j}\right] + 2(1 - F_1)\sigma_{\omega^2}\frac{1}{\omega}\frac{\partial k}{\partial x_i}\frac{\partial \omega}{\partial x_i} \qquad (4)$$

The Incompressible Navier-Stokes Equations in a Moving Reference Frame with Absolute Velocity can be written as below.

$$\frac{\partial u_0}{\partial t} + \frac{d\omega_2}{dt} \times r + \nabla.(u_2 \otimes u_0) + \omega_2 \times u_0 = -\nabla\left(\frac{p}{\rho}\right) + v\,\nabla.\nabla u_0 \qquad (5)$$

$$\frac{\partial u_0}{\partial t} + \frac{d\omega_3}{dt} \times r + \nabla.(u_3 \otimes u_0) + \omega_3 \times u_0 = -\nabla\left(\frac{p}{\rho}\right) + v\,\nabla.\nabla u_0 \qquad (6)$$

where,

Convection term is of the form ($\nabla.(u_2 \otimes u_0)$)

The convection velocity is the velocity u_2 & u_3 relative to the moving reference frame and u_0 is velocity the laboratory frame that is absolute velocity (STAR CCM+ 11 User Guide).

Equation (5) and (6) gives the momentum equation in the moving reference frame denoted by co-ordinate axes X_2, Y_2, Z_2 and X_3, Y_3, Z_3 with the absolute velocity formulation that is for the rotation of the cylinder and the rotation of rotor blade respectively as shown in figure 11.

2.2. Numerical Method Validation

Simulations with the isolated ship and isolated rotor and their coupling are performed here to signify the effectiveness of this method as there is a lack of experimental data for ship rotor coupled flow field. The simulation of the rotor in out of ground effect (OGE) is also done to support the validation.

2.2.1. Ship in Isolation

In the simulations, the SFS model is used as experimental geometry for it is available. The calculation is carried out with a relative velocity of V_∞= 20 m/s for a headwind. The comparisons of time-averaged streamwise velocity distributions is made between the experimental data shown in figure 3 [14] and the CFD calculation over the flight deck in figure 4. It can be observed from figure 3 & 4 that the computed results agree well with the experimental measurements. PIV measurements indicate a re-attachment location of 2.5h of the hangar on the centreline of flight deck, where h is the hangar height [14]. The CFD calculation shows that the reattachment occurs at approximately 2.45 times the hangar height, which predicts the margin of error in CFD results is very less as compared to the experimental data.

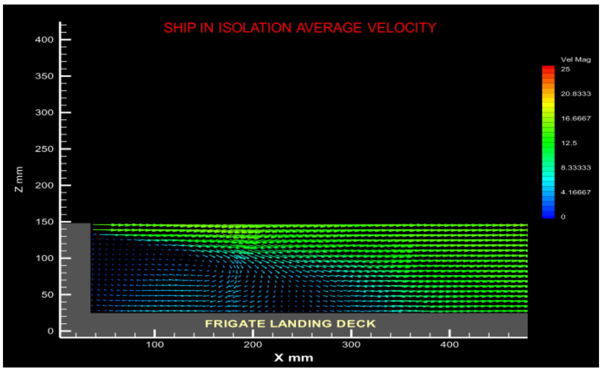

Figure 3: PIV velocity flowfield for the ship in isolation with reattachment at 2.5h.[14]

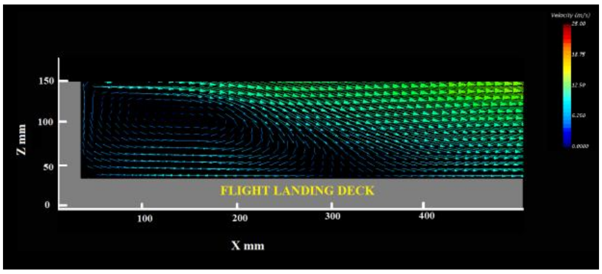

Figure 4: CFD velocity flowfield for the ship in isolation with reattachment at 2.45h.

Presented at 45th European Rotorcraft Forum, Warsaw, Poland, 17-20 September, 2019

2.2.2. The rotor in Isolation

The experimental data of the rotor in the OGE condition used here is provided by Y. Nacakli [14]. This experimental setup consists of a four-bladed rotor with a diameter of 0.25m and at a total pitch of 0.15m. Figure 5 and Figure 6 shows the comparisons between the computed and the measured mean thrust for an advance ratio of 0.075 with a rotor speed of 5000 rpm. It can be observed that the thrust coefficient of the rotor is computed to be 0.01156 with an error of 7% from the experimental value.

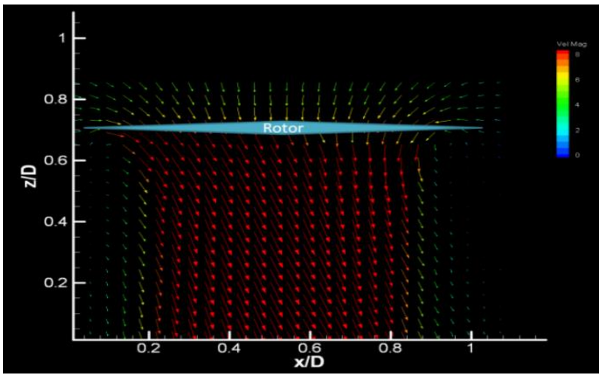

Figure 5: PIV velocity flowfield ($K_T = 0.01087$) [14]

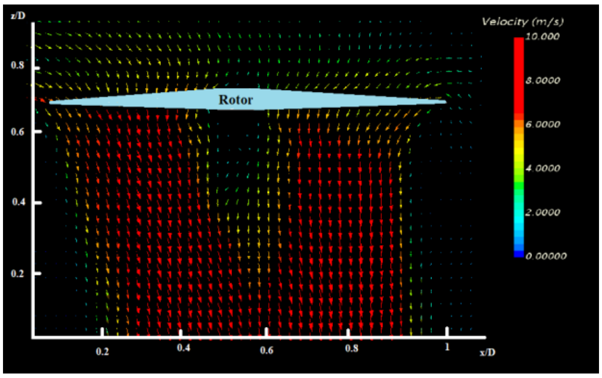

Figure 6: CFD velocity flowfield ($K_T = 0.01156$)

Furthermore, to analyse grid independence, the constructed grids have a cell growth rate of √2. The target cell sizes (Δ) around the ship are 6×10^{-3} m, 4.24×10^{-3} m and 3×10^{-3} m and refined mesh consists of approximately 4.1, 4.5 and 5.2 million cells respectively. The error in the measurement of thrust coefficient between 5.2 and 4.5 million cells is less than 1% and so it can be stated that the grid independence has been achieved as shown in figure 7.

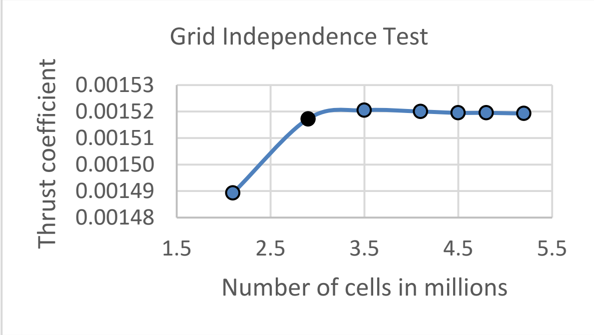

Figure 7: Grid Independence test for rotor at K-plane with the base model (SFS2)

2.2.3. Numerical Set-up and Data Analysis

A 1:100 scale SFS2 as shown in figure 8 [12] is chosen for this study because this model represents characteristics of both geometric realism and mesh complexity, and its airwake generally reflects the typical flow features of a frigate over the flight deck. The ROBIN fuselage (figure 10) is a simplified helicopter fuselage proposed by NASA for helicopter fuselage study [15].

Table 1: Ship and Rotor-Blade Dimensions

1:100 SFS2 (mm)		Rotor Blade (mm)	
Deck-Length	280	No. of Blades	3
Ship Beam	140	Diameter	177.8
Hangar height(h)	63	Pitch	76.2

In general, there are two or more landing spots on the flight deck for an amphibious landing ship for the shipboard operation of helicopters [6]. This study is carried out for one landing spot located at 50% of the flight deck length behind the hangar on the centreline of the SFS2 as shown in figure 8. The rotor helicopter is located at 2 points along the vertical descent paths as shown in figure 8. At each rotor position the calculation is done for a headwind of $V_\infty = 6\ m/s$.

A rectangular computational domain [12,15] is generated by the STAR CCM+ 11 (figure 9), where L is the length of SFS2. The dimensions are as below :

Computational Domain	Dimensions
Length	6L
Width	0.55L
Height	0.35L
Blockage effect	5~6%

Presented at 45th European Rotorcraft Forum, Warsaw, Poland, 17-20 September, 2019

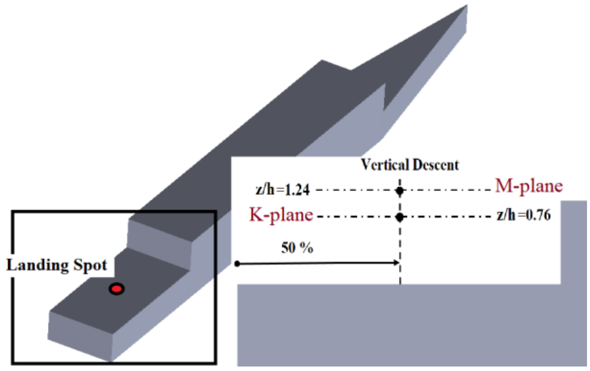

Figure 8: A 1:100 scaled SFS2 model with 2 rotor locations along vertical descent paths relative to the flight deck [6]

The inlet and outlet boundaries are specified as velocity inlet and pressure outlet, respectively, and the ship body is designated to have a no-slip condition [6,12,15]. The boundary conditions in detail are tabulated in table 2. The Robin body, the rotor blades and the ship surface are extruded with prism layer mesh in order to capture the boundary layer as shown in figure 10. Sliding Plane mesh technique allows the rotation of the blade and the cylinders (figure 11). The grids on the blade surface and the rotating cylinder are refined with a target cell size of 0.06 mm to improve the vortex preservation. Thereafter, two interfaces are created between the background mesh and the blade rotating mesh and between the background mesh and the rotating cylinder mesh. This interpolated algorithm is then used to exchange information between the two types of grids as discussed, thus illustrating the two-way coupling in the ship-rotor simulation [6].

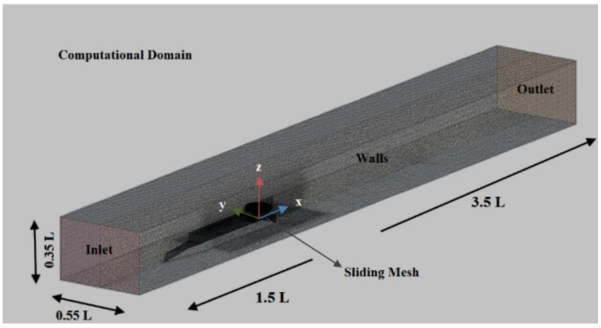

Figure 9: Computational domain (IIT Delhi Low-speed wind tunnel Test-Section)

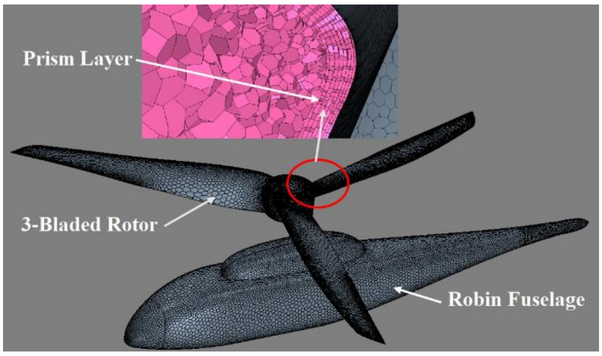

Figure 10: Fine mesh and Prism layer on Robin-fuselage and 3-bladed rotor

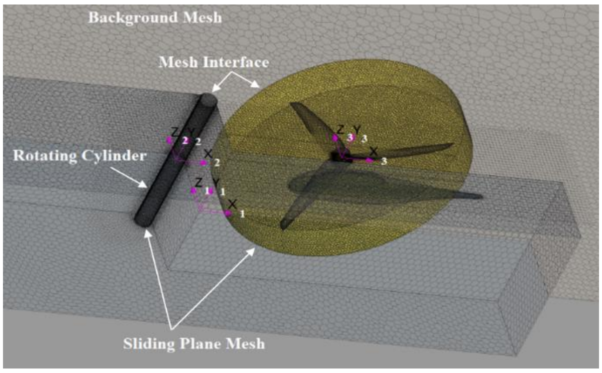

Figure 11: Sliding Plan and Mesh Interface between background and rotating mesh

Table 2: Details of Boundary Conditions

<table>
<tr><td>Parameters</td><td>Stationary-Region
Boundary Conditions</td><td>Rotating Region
Boundary Conditions</td></tr>
<tr><td>Inlet</td><td>$V_\infty = 6\, m/s$,
Turbulent Specifications;
Intensity=1%, Velocity Sale=10% of free stream velocity(V_∞).</td><td rowspan="2">The rotating reference frame is used for Rotation of rotor-blade (X_3,Y_3,Z_3) and Cylinders (X_2,Y_2,Z_2).
The blade Rotation rate is 5000 rpm, and for the cylinder is tabulated below:
<table>
<tr><th>d/h</th><th>β</th><th>Ω (rpm)</th></tr>
<tr><td>Base-model</td><td>-</td><td>-</td></tr>
<tr><td>0.14</td><td>1.1</td><td>14291.5</td></tr>
<tr><td>0.2</td><td>1.6</td><td>14551.3</td></tr>
<tr><td>0.24</td><td>1.95</td><td>14800.0</td></tr>
</table></td></tr>
<tr><td>Outlet</td><td>Pressure Outlet
Backflow Turbulent Specifications:
Intensity=1%, Velocity scale=10% of free stream velocity(V_∞).</td></tr>
<tr><td>Domain Walls</td><td>Stationary Wall with zero specified shear (Figure 9)</td><td>Rotating Part Wall is Stationary, with no slip condition</td></tr>
<tr><td>SFS-2, ROBIN & Rotor- blade</td><td colspan="2">Stationary wall with no-slip condition</td></tr>
<tr><td>Discretization Method</td><td colspan="2">Turbulence model standard $k-\omega$ model
Momentum, Turbulent Kinetic energy & Dissipation rate: Second order Up-Wind method</td></tr>
</table>

3. RESULTS AND DISCUSSIONS

3.1. Recirculation Length

Figure 12 represents the line integral of the recirculation length for various velocity ratios (β) on the centerline plane over the flight deck. For β=0 (i.e. stationary cylinder), the reattachment of flow occurs at 62% of the length of the flight deck from the hangar door (figure 12(a)). It can be observed that if rotation is given to the cylinder installed at the top edge of hangar door, the flow starts to curl more towards the hangar door, which results in a decrease in the recirculation length. For β=1.1 as shown in figure 12(b) the reattachment length is approximately 54% of the length of the flight deck and for a higher value of β=1.6, the flow attaches at the 52% of deck length. It can be observed that there is almost 4% decrease in the recirculation length in case of β=1.95 in comparison with β=1.6 (figure 12(c) and 12(d)).

The inference obtained is, as the diameter of the cylinder increases the reattachment of flow occurs at a shorter length of the flight deck.

Presented at 45th European Rotorcraft Forum, Warsaw, Poland, 17-20 September, 2019

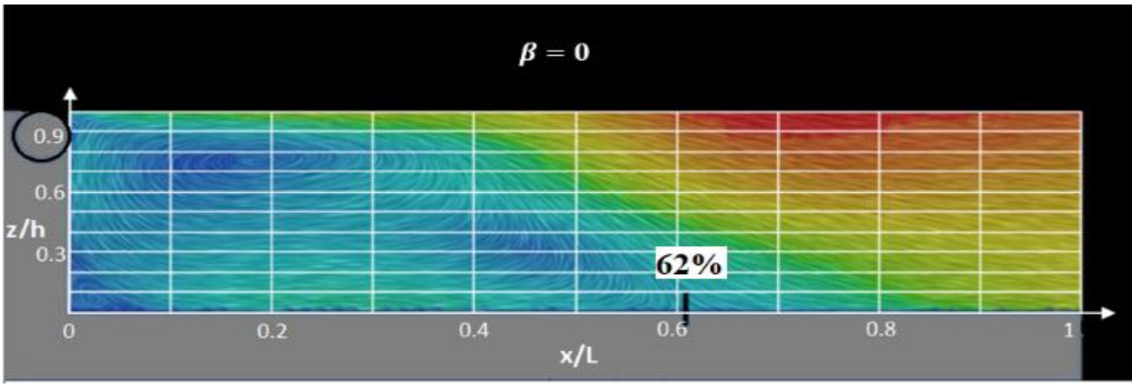

Figure 12 (a) Recirculation length for cylinder without rotation on centreline plane

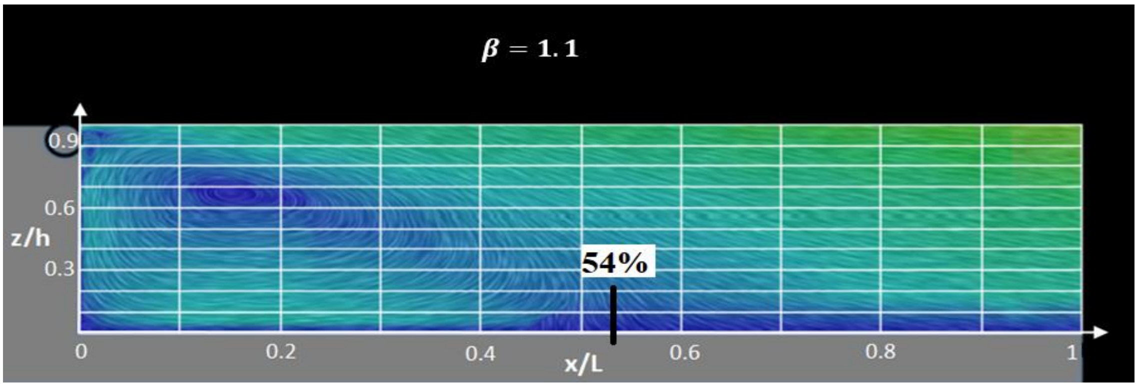

Figure 12(b) Recirculation length for β=1.1 on centreline plane

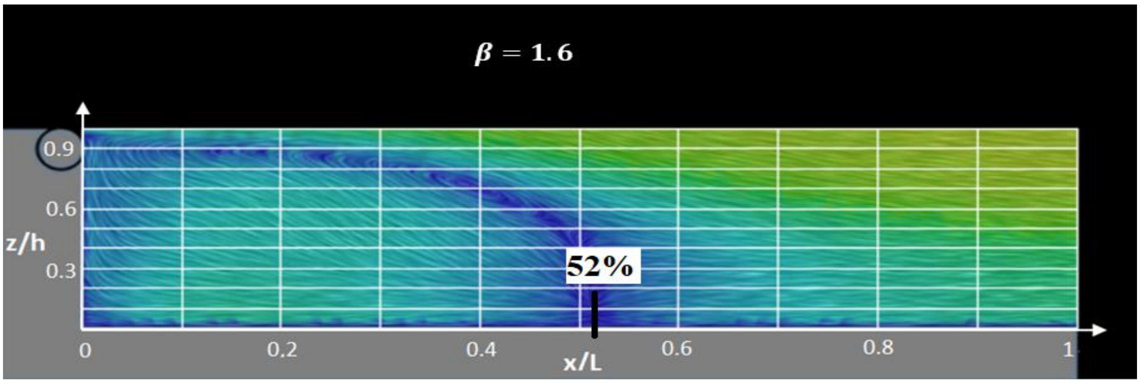

Figure 12 (c) Recirculation length for β=1.6 on centreline plane

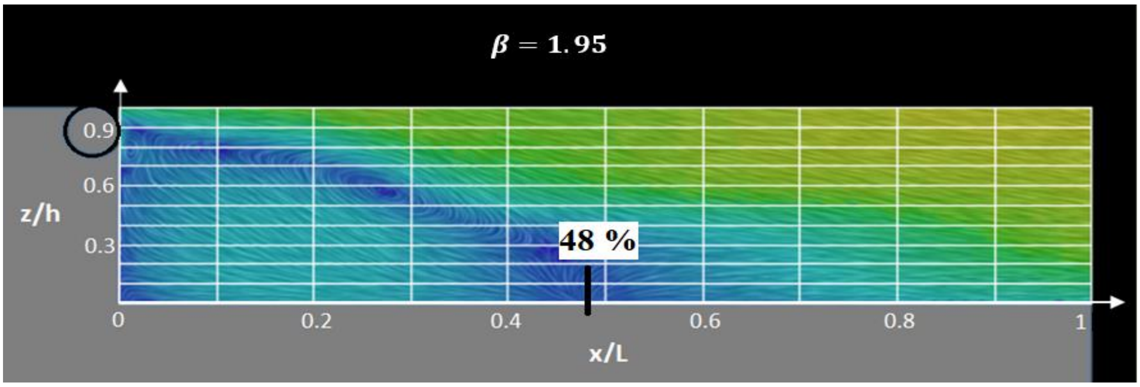

Figure 12(d) Recirculation length for β=1.95 on centreline plane

Presented at 45th European Rotorcraft Forum, Warsaw, Poland, 17-20 September, 2019

3.2. Thrust Coefficient

The thrust coefficient of a helicopter rotor is calculated using the formula given below:

$$K_T = \frac{T}{\rho n^2 D^4} \quad (7)$$

where,

T Thrust generated by the rotor (N)
ρ Density of air (1.225 $kg\ m^{-3}$)
n Rotation rate ($rad\ s^{-1}$)
D Diameter of the rotor blade

The rotor thrust coefficient is calculated for the base model i.e. SFS2 and 3- different cylinder diameters each with a different velocity ratio, which is tabulated below:

Table 1: Thrust Coefficient at K and M plane

d/h	β	Ω (RPM)	K_T (10^{-3})	
			K-plane	M-plane
Base-model	-	-	1.29	1.52
0.14	1.1	14291.5	1.32	1.49
0.2	1.6	14551.3	1.34	1.44
0.24	1.95	14800.0	1.36	1.41

Figure 13 shows the variation of thrust coefficient with the velocity ratio β over the longitudinal centreline plane perpendicular to the flight deck for both the rotor positions – at K and M-planes.

When the rotor is located at $z/h = 0.76\ (K-Plane)$, it is observed that the thrust coefficient increases as the velocity ratio is increased (i.e. the diameter of the cylinder is increased) as represented in figure 13. On the contrary, it decreases with an increase in the velocity ratio when the rotor is positioned at $z/h = 1.24\ (M-Plane)$. This is because, by installing rotating cylinder on the top edge of hangar, the separation of flow gets delayed and occurs at the farther aft and downwards on the cylindrical surface as compared to the base model in which the separation of flow occurs as soon as the air leaves the top edge of the hangar. This results in increased momentum of air flowing inside the wake region and results in a subsequent decrease in the recirculation length as represented in figure 12(a) to (d).

Furthermore, another observation deduced from the study is that as the position of rotor-blade is shifted upwards in the Z_1 X_1 plane (i.e. from K to M-plane) the thrust coefficient corresponding to every value of velocity ratio is more for M-plane which again justifies the theory that for the same hangar geometry the momentum of air flowing is more on the plane which is far from the wake region owing to the higher velocity of air flow in that region. This higher velocity is close to free stream velocity of the flow field.

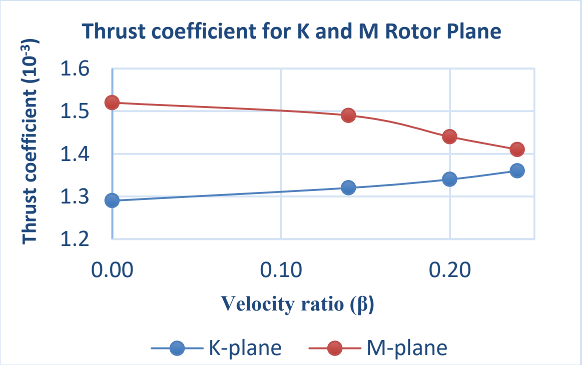

Figure 13 Thrust-coefficient 'vs' Velocity ratio

3.3. Turbulence intensity

The numerical calculation of turbulence intensity is performed in STAR CCM + using the user defined formula as given below:

$$I = \frac{\sqrt{\frac{2}{3}k}}{V_0} \quad (8)$$

k Turbulent Kinetic energy

V_0 Instantaneous cell velocity

The rotor when hovering at position z=48 mm i.e. z/h=0.76 marked as K-plane, the turbulent intensity is measured at five different planes on the centerline plane perpendicular to the flight deck marked in figure 14 (a). The following plots in figure 14 (b) to 14 (f) shows the variation of turbulence intensity along the length of the flight deck for four different geometric specifications of ship hangar with and without rotating cylinder of varied diameters as labeled below.

Presented at 45th European Rotorcraft Forum, Warsaw, Poland, 17-20 September, 2019

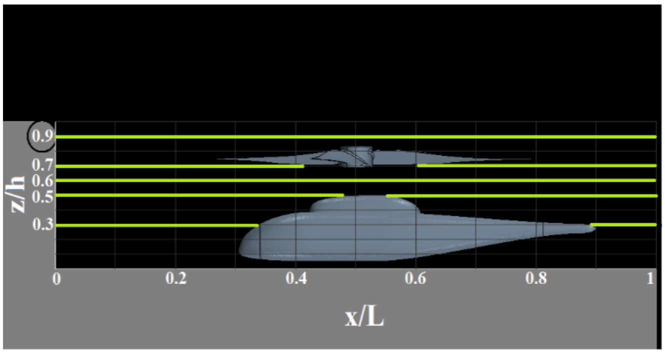

Figure 14(a) Positions for measurement of turbulence intensity at the centerline plane at various heights z when the rotor is at z=48 mm (K-Plane)

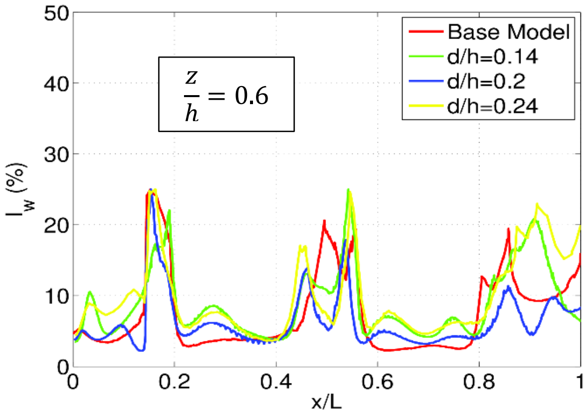

Figure 14(d) Variation of turbulence intensity at height z=37.8 mm for rotor positioned at K-plane

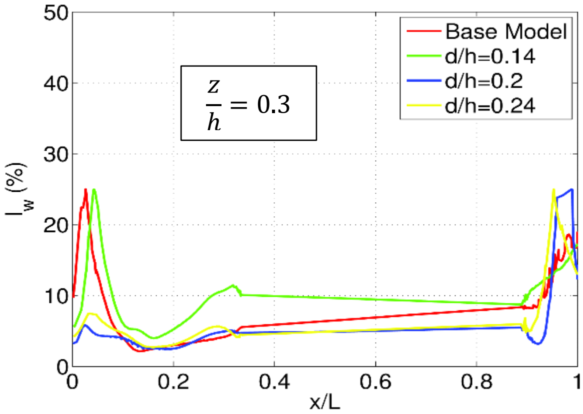

Figure 14(b) Variation of turbulence intensity at height z=18.9 mm for rotor positioned at K-plane

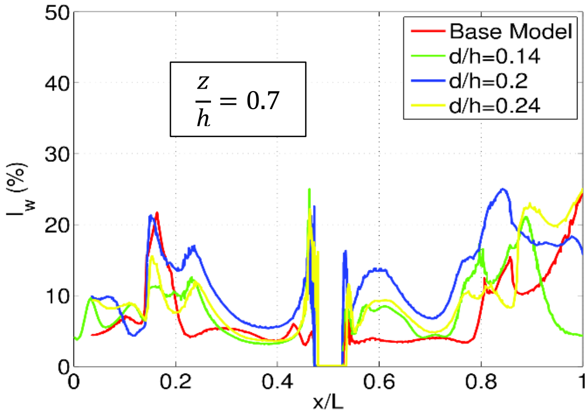

Figure 14(e) Variation of turbulence intensity at height z=44.1 mm for rotor positioned at K-plane

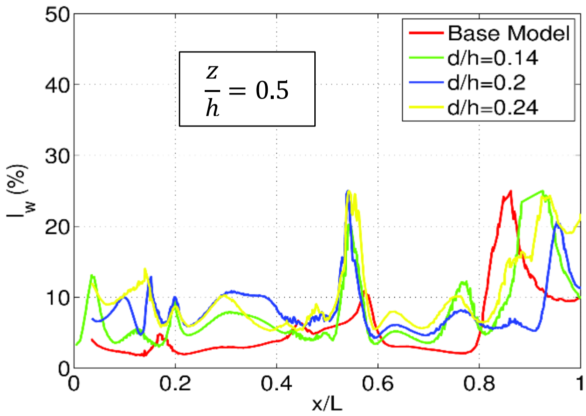

Figure 14(c) Variation of turbulence intensity at height z=31.5 mm for rotor positioned at K-plane

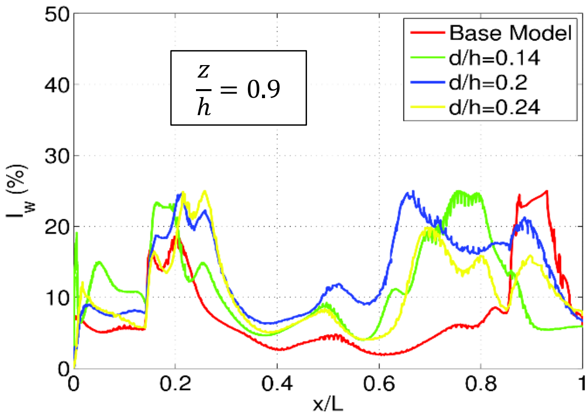

Figure 14(f) Variation of turbulence intensity at height z=56.9 mm for rotor positioned at K-plane

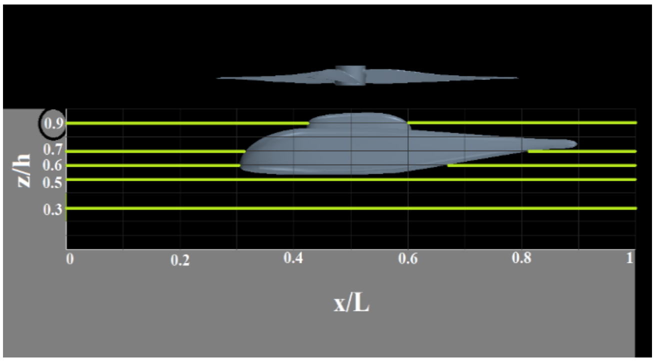

Figure 15(a) Positions for measurement of turbulence intensity at the centerline plane at various heights z when the rotor is at z=78 mm (M-plane)

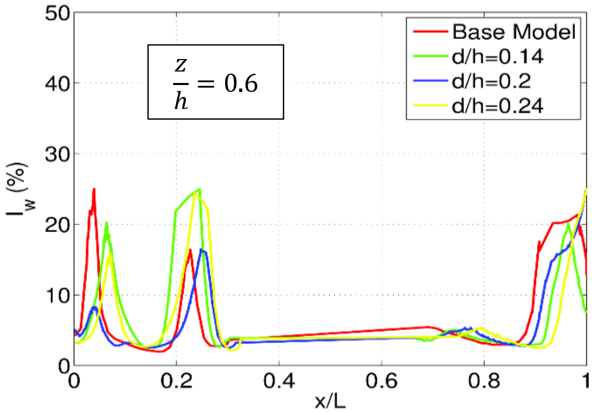

Figure 15(d) Variation of turbulence intensity at height z=37.8 mm for rotor positioned at M-plane

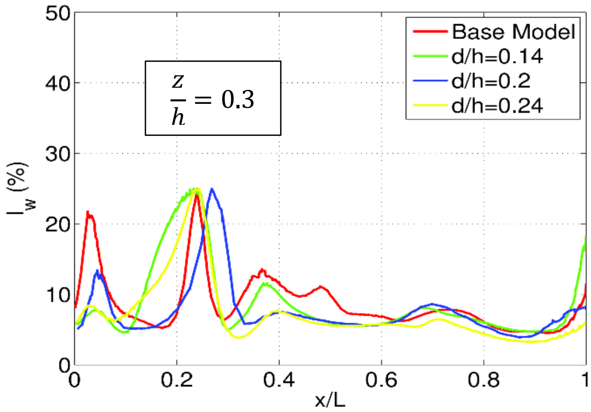

Figure 15(b) Variation of turbulence intensity at height z=18.9 mm for rotor positioned at M-plane

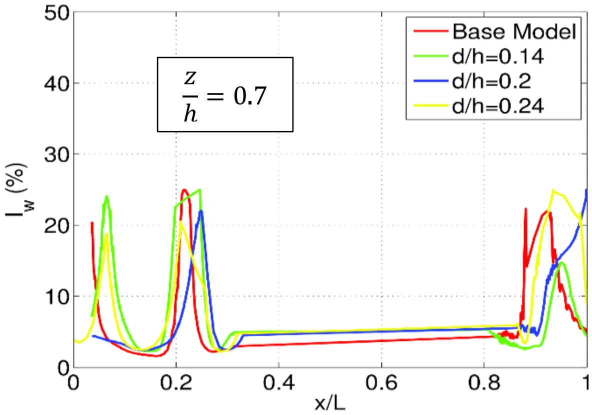

Figure 15(e) Variation of turbulence intensity at height z=44.1 mm for rotor positioned at M-plane

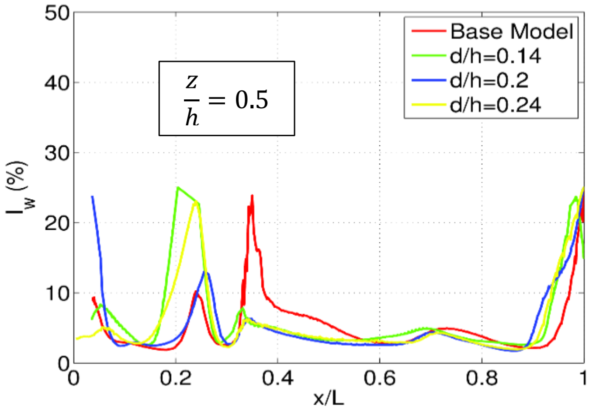

Figure 15(c) Variation of turbulence intensity at height z=31.5 mm for rotor positioned at M-plane

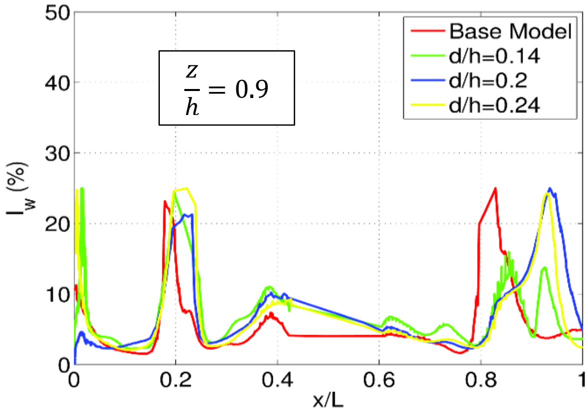

Figure 15(f) Variation of turbulence intensity at height z=56.9 mm for rotor positioned at M-plane

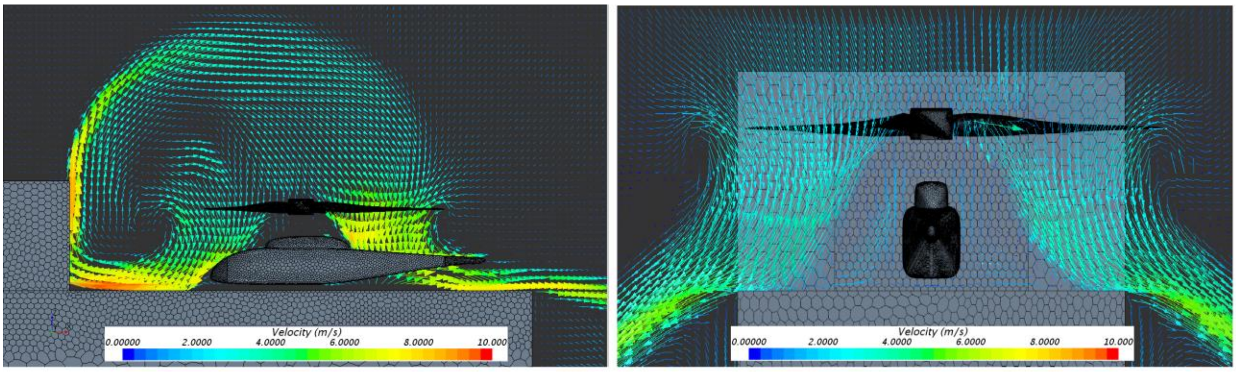

Figure 16 (a) Visualization of velocity of flowfield for base model when rotor at K-plane

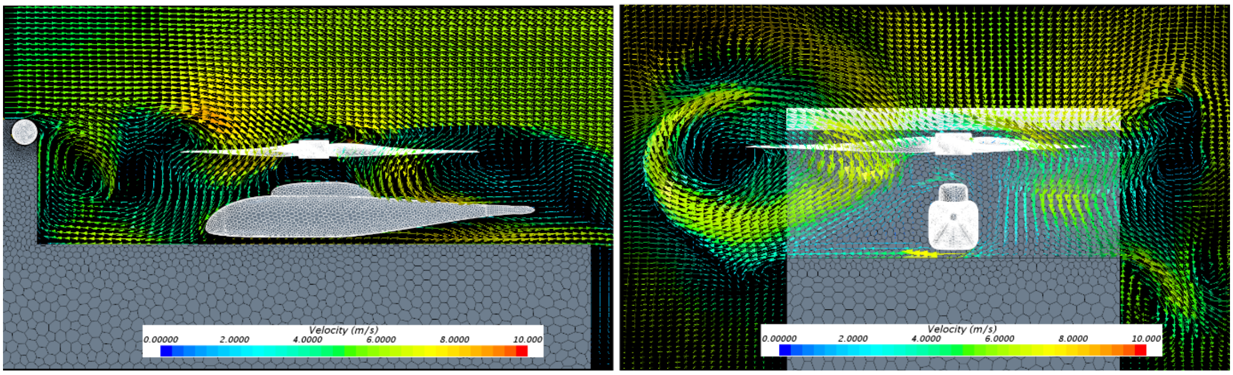

Figure 16 (b) Visualization of velocity of flowfield for ship hangar equipped with rotating cylinder when rotor at K-plane

The turbulent intensity can be observed to be higher than 5 % over the flight deck for all heights and also for both rotor positions, at K and M-plane, the flow is thus considered to be highly turbulent in nature. A peak in the value of turbulence intensity is observed near the hangar door i.e. at x/L nearly zero which is a result of the sudden drop in the velocity magnitude because of the ship airwake (Figure 14). In the two cases, firstly for the base model and secondly for the smallest cylinder diameter (d/h=0.14) with the lower velocity ratio (β=1.1) the turbulence intensity is higher close to the hangar door. Local peaks are observed in the value of turbulence intensity near to x/L = 0.23 and x/L=0.9 i.e. the downstream of the Robin fuselage, due to the formation of wing tip vortices and blade vortex interaction (BVI) owing to the presence of tip of the rotor blade at x/L=0.8 downstream and x/L=0.2 upstream. Moreover, the location just below the rotor blade shows a peak in turbulence at half-length of the flight deck that is because of the flushing of vortices from the blade tip towards the tail of fuselage and because of the downdraft of the blade. It can be observed that turbulence intensity is higher in case of a larger cylinder and less in the base model. Also, the blank space in the graph (figure 14(b), (e) and figure 15(d), (e) & (f)) represent the presence of a solid body (Robin-fuselage or rotor blade) on which the turbulence is marked as zero.

For the rotor position at K as well as M-plane, on an average, the base model has the lowest turbulence for all values of z/h (figure 14 and 15). The visualization of flow as seen from the distribution of velocity in the air flow field when the rotor position is at K-plane (figure 16 (a) and (b)) illustrates the fact that by installing a rotating cylinder at the edge of the hangar the fluctuations in velocity increases and thereby the turbulence behind the hangar also increases. The similar results are replicated even when the rotor is shifted upwards at M-plane and irrespective of the diameter of cylinder the turbulence is more in case of the modified hangar configuration than that in the base model. The modified SFS2 with cylinders is observed to have a similar trend out of which more turbulence can be observed for higher velocity ratio (β=1.95) followed by that for β=1.6 and further β=1.1.

4. CONCLUSIONS

In order to carry out safe marine aviation operations a study of operations from helo-decks of ships – considering the complex coupled flow behavior on the helo-deck during helo

Presented at 45th European Rotorcraft Forum, Warsaw, Poland, 17-20 September, 2019

landing/take-off is essential. For that matter, the current research involved RANS simulations for understanding the coupled behavior of a helicopter fuselage and ship airwake in the presence of a rotor downwash. The simulations involved an airwake resulting from the propulsion of a simplified ship: SFS2, downwash generated by a 3-bladed helicopter rotor and a simplified helicopter fuselage: ROBIN fuselage. The simulations are carried out to assess the coupling effects of airflow on the flight deck using STAR CCM+ code based upon FVM (Finite Volume Method) solver. This solver solves RANS (Reynolds-Averaged-Navier-Stokes) equation along with the two-equation $k-\omega$ turbulence model as a CFD tool. Available experimental data was used to validate the numerical simulations in the first phase of the study.

Following inferences can be obtained from this study:

It can be concluded from all the results that the coupled flow characteristic is majorly influenced by the velocity ratio (β). For instance, as the velocity ratio increases the reattachment of flow over the flight deck occurs early. Hence the recirculation length has reduced by 14 percent for a frigate equipped with a cylinder of diameter to height ratio of 0.24 as compared to that of the base model. Another direct result of which is the reduction of the volume of wake region behind the hangar as seen in figure 12(a) to 12(d). The reduced airwake can prove advantageous in decreasing the pilot workload and make the conditions for HELO safer.

Secondly, the thrust coefficient is also a function of velocity ratio along with the rotor position owing to which the thrust increases as the velocity ratio increases when the rotor is at K-plane which is close to the flight deck while it reduces with the velocity ratio for rotor positioned at more height from the deck i.e. at M-plane.

The observations for turbulence intensity so derived infers that the prediction of turbulence is very difficult for the case of coupled flow due to ship airwake and helicopter downwash. The turbulence is less in case of the base model and shows a non-uniform variation for all the other three models. This study can help to get a trend of turbulence intensity showing the probable locations of peaks and drops but it does not prove to be effective for quantifying turbulence intensity at every location accurately. While this research does not provide an explicit variation of turbulence intensity it still can be used to set up a basic platform to predict the accurate variation of turbulence intensity further by employing other numerical or experimental techniques.

To carry out safe HELO in naval operations it is very important to have a good knowledge and understanding of flow condition over the flight deck. This study serves an effective tool to enhance the understanding of the highly unsteady, turbulent and complex coupled air flowfield. The approach used here helps to find out a way to appropriately quantify key parameters like recirculation length and thrust coefficient while establishes a trend for turbulence intensity at various locations on the flight deck for the corresponding location of helicopter rotor and fuselage. Adopting such modifications in the configuration of frigate hangar can directly help in decreasing the adverse effects of the coupled complex air wake and hence indirectly reduce the pilot workload.

5. REFERENCES

[1] Wikipedia contributors, "Shipboard helicopter operations," *Wikipedia,The Free Encyclopedia,* https://en.wikipedia.org/w/index.php?title=Shipboard_helicopter_operations&oldid=829333160 (accessed July 29, 2019).

[2] Thornber B, Starr M, Drikakis D. Implicit large eddy simulation of ship airwakes. The Aeronautical Journal. 2010 Dec;114(1162):715-36.

[3] Leishman, J.L., Principles of Helicopter Aerodynamics, Cambridge University Press, 2001.

[4] Crozon C, Steijl R, Barakos GN. Numerical study of helicopter rotors in a ship airwake. Journal of Aircraft. 2014 Aug 12;51(6):1813-32.

[5] Saleel CA, Shaija A, Jayaraj S. Computational simulation of fluid flow over a triangular step using immersed boundary method. International Journal of Computational Methods. 2013 Aug 12;10(04):1350016.

[6] Su D, Xu G, Huang S, Shi Y. Numerical investigation of rotor loads of a shipborne coaxial-rotor helicopter during a vertical landing based on moving overset mesh method. Engineering Applications of Computational Fluid Mechanics. 2019 Jan 1;13(1):309-26.

[7] Vijayakumar R. Study on the interaction of exhaust smoke with the superstructure and gas turbine intakes of naval ships(Doctoral dissertation).

[8] Crozon C, Steijl R, Barakos GN. Coupled flight dynamics and CFD–demonstration for helicopters in shipborne environment. The Aeronautical Journal. 2018 Jan;122(1247):42-82.

[9] Shukla S, Sinha SS, Singh SN. Ship-helo coupled airwake aerodynamics: A comprehensive review. Progress in Aerospace Sciences. 2019 Mar 5.

[10] Forrest JS, Kääriä CH, Owen I. Determining the Impact of Hangar-Edge Modifications on–Ship–Helicopter Operations using Offline and Piloted Helicopter Flight Simulation. InAmerican Helicopter Society 66th Annual Forum 2010 May 11 (Vol. 3, pp. 11-13).

[11] Wang J, Jiang G, Wang X. Effect analysis of the hangar rear edge curvature on the ship airwake. InIOP Conference Series: Materials Science and Engineering 2018 Aug (Vol. 408, No. 1, p. 012024). IOP Publishing.

[12] Praveen B. Study of the ship airwake helodeck flow field for safe helo operations (Doctoral dissertation).

[13] Salim SM, Ong KC, Cheah SC, Ntroduction II. Comparison of RANS, URANS and LES in the prediction of airflow and pollutant dispersion. InProceedings of the world congress on engineering and computer science 2011 Oct 19 (Vol. 2, pp. 19-21).

[14] Nacakli Y, Landman D. Helicopter downwash/frigate airwake interaction flowfield PIV surveys in a low speed wind tunnel. InAnnual Forum Proceedings of the American Helicopter Soc 2011 May (Vol. 4, pp. 2988-2998).

[15] S. Shukla, I.S. Makkar, S.N. Singh , S.S. Sinha and R. Vijayakumar, Numerical studies of coupled flow effects due to ship airwake and rotor downwash interaction on warship helo-decks, International Conference of Ocean Engineering, Royal Institute of Naval Architects, 2017.

Presented at 45th European Rotorcraft Forum, Warsaw, Poland, 17-20 September, 2019

APPENDIX A

ABBREVIATIONS:

SFS	: Simplified-Frigate-Ship
FVM	: Finite Volume Method
RANS	: Reynolds-Averaged-Navier-Stokes
CFD	: Computational Fluid Dynamics
WOD	: Wind over deck angle
DI	: Dynamic Interface
DES	: Detached Eddy Simulation
LES	: Large Eddy Simulation
LHA	: Landing Helicopter Assault
MILES	: Monotone Integrated Large Eddy Simulation
URANS	: Unsteady Reynolds-Averaged-Navier-Stokes
OGE	: Out of ground effect
Rpm	: Rotation per minute
ROBIN	: Rotor-Body-Interaction
HELO	: Helicopter Operations

SYMBOLS :

K_T	: Thrust Coefficient
u_2	: relative velocity of moving reference frame (cylinder)
u_3	: relative velocity of moving reference frame (rotor-blade)
u_0	: absolute velocity
$\boldsymbol{\omega}_2$	: angular velocity of cylinder
$\boldsymbol{\omega}_3$	: angular velocity of rotor blade
r	: position vector from origin of moving reference frame
h	: Hangar Height
β	: velocity ratio
Δ	: Cell size
Ω	: rotation rate in rpm
V_0	: Absolute cell velocity
x/L	: Flight Deck length Ratio

Presented at 45th European Rotorcraft Forum, Warsaw, Poland, 17-20 September, 2019